Noncontact Impedance Control for Redundant Manipulators

Toshio Tsuji and Makoto Kaneko

***Abstract*—This paper proposes an impedance control method that can regulate a virtual impedance between a robot manipulator and external objects using visual information. The conventional impedance control method is not useful in some cases where no interaction force between the arm and its environment exists, although it is one of the most effective control methods for manipulators in contact with the environment. Using the proposed method, we can control the manipulator motion based on the virtual impedance before contact with the objects. The validity of the proposed method is verified through computer simulations and experiments using a direct-drive robot.**

***Index Terms*—Impedance control, manipulators, motion-planning, redundancy, robot dynamics, robot vision systems.**

I. Introduction

IMPEDANCE control is a method to regulate the mechanical impedance of an end-effector of a robot manipulator in a desired value according to a given task. It can specify the desirable response of the end-effector for an external force. Hogan [1] invented a method to control the end-effector impedance of a manipulator based on the measured position, velocity and force of the end-effector. Since then, many studies have been conducted, including realization techniques [2], [3] and stability analysis for contact motion [4]. The impedance control is one of the most important frameworks to control the interaction between the manipulators and the environment.

In some cases, however, the occurrence of an interaction force between a manipulator and its environment needs to be carefully considered. For example, when the end-effector grasps a fragile object, the approaching velocity of the end-effector should be decreased before coming into contact with the object in order to prevent a large impact force. Also in environments with obstacles, the interaction force between the obstacle and the manipulator should be avoided. Under the conventional impedance control method, it is difficult to cope effectively with such situations, since no external force is exerted until the end-effector makes contact with objects.

In other cases, vision-based control for robot manipulators has been actively exploited in recent years [5]–[7], where the robot is controlled according to the visual information on the task space. Based on the framework of vision-based control, Castano and Hutchinson [8] proposed the concept of visual compliance. This method can constrain the end-effector motion on a virtual task plane based on a hybrid control by using both the visual sensor information from a camera system and the joint angular information from encoders attached at the joints of the manipulator. However, it does not control the impedance itself based on visual information.

For impedance control using visual information, only a few methods have been proposed thus far. Arai *et al*. [9] have proposed a concept of virtual impedance for the motion planing of multiple mobile robots. In this method, the virtual impedances among the robots, the goal and the obstacles are defined and virtual forces resulting from the virtual impedances are utilized in order to achieve coordinated control of the multiple mobile robots. For manipulators, we proposed a vision-based impedance control [10], [11] using virtual impedance, which can control virtual impedance between the end-effector and the object in addition to the end-effector's impedance. Nakabo *et al.* [12] have also proposed a concept of visual impedance and were able to show that the movement of the end-effector can be modified in real time (less than 1 ms sampling time) by using the visual impedance between the end-effector and the object. In these methods, however, the relative arm motion to the object is controlled for only by the objects approaching the end-effector.

In this paper, we apply the vision-based impedance control to a redundant manipulator and thus propose a noncontact impedance control which can utilize kinematic redundancy [13]. This method can control the virtual impedance between the object and multiple points set on the arm, including the end-effector, so that the virtual interaction between the whole arm and the environment can be considered. Additionally, we discuss how the virtual impedance parameters can be designed in consideration to the overall control properties of the system.

This paper is organized as follows: In Section II, the impedance control of a manipulator is briefly explained, with an emphasis on the utilization of redundant joint degrees of freedom; next, the noncontact impedance control is formulated for a redundant manipulator in Section III; and in Sections IV and V, computer simulations and experiments are performed in order to make clear the distinctive feature of the proposed method.

II. Impedance Control

In general, a motion equation of an m-joint manipulator can be expressed as

$$M(\theta)\ddot{\theta} + h(\theta, \dot{\theta}) = \tau + J^T(\theta)F_{\text{ext}} \tag{1}$$

Manuscript received October 1, 1997; revised September 18, 1998.

The authors are with the Department of Industrial and Systems Engineering, Hiroshima University, Higashi-Hiroshima, 739-8527 Japan (e-mail: tsuji@huis.hiroshima-u.ac.jp).

Publisher Item Identifier S 1083-4427(99)01449-6.

where $F_{\text{ext}} \in \Re^l$ is the external force exerted to the end-effector; $\theta \in \Re^m$ is the joint angle vector; $M(\theta) \in \Re^{m\times m}$ is the nonsingular inertia matrix (hereafter denoted by M); $h(\theta,\dot\theta) \in \Re^m$ is the nonlinear term including the joint torque due to the centrifugal, Coriolis, gravity and friction forces; $\tau \in \Re^m$ is the joint torque vector; $J(\theta) \in \Re^{l\times m}$ is the Jacobian matrix (hereafter denoted by J); and l is the dimension of the task space. For a redundant manipulator, m is larger than l.

The desired impedance of the end-effector is described by

$$M_e d\ddot X + B_e d\dot X + K_e dX = F_{\text{ext}} \tag{2}$$

where $M_e, B_e, K_e \in \Re^{l\times l}$ are the desired inertia, viscosity and stiffness matrices of the end-effector, respectively; and $dX = X - X_d \in \Re^l$ is the displacement vector between the current end-effector position X and the desired one (namely, the equilibrium position of the end-effector) X_d.

In this paper, we adopt the impedance control law without using an inverse of the Jacobian matrix presented in [2]

$$\tau = \tau_{\text{effector}} + \tau_{\text{comp}} \tag{3}$$

$$\tau_{\text{effector}} = -J^T\big[M_x(\theta)\big\{M_e^{-1}(K_e\, dX + B_e d\dot X + \dot J\dot\theta - \ddot X_d\big\} + \big\{I - M_x(\theta)M_e^{-1}\big\}F_{\text{ext}}\big] \tag{4}$$

$$\tau_{\text{comp}} = (\bar J J)^T \hat h(\theta,\dot\theta) \tag{5}$$

where $M_x(\theta) = (J\hat M^{-1}J^T)^{-1} \in \Re^{l\times l}$ is the operational space kinetic energy matrix [14], [15]; $\bar J = \hat M^{-1}J^T M_x(\theta) \in \Re^{m\times l}$ is the generalized inverse of J weighted by $\hat M^{-1}$; $\tau_{\text{effector}} \in \Re^m$ is the joint torque vector needed to produce the desired end-effector impedance; I is the $l\times l$ unit matrix; $\tau_{\text{comp}} \in \Re^m$ is the joint torque vector for nonlinear compensation; and $\hat h(\theta,\dot\theta)$, $\hat M$ are the estimated values of $h(\theta,\dot\theta)$ and M. It is assumed that $\hat h(\theta,\dot\theta) = h(\theta,\dot\theta)$, $\hat M = M$, and the joint configuration θ is not in a singular posture.

Although the control law (3)–(5) or other impedance control methods such as [1], [3] can be applied to control redundant manipulators, they cannot effectively utilize arm redundancy. In order to exploit the arm redundancy, an additional controller for a subtask needs to be incorporated into the end-effector impedance control system in parallel [16], [17]

$$\tau = \tau_{\text{effector}} + \tau_{\text{comp}} + \tau_{\text{joint}} \tag{6}$$

$$\tau_{\text{joint}} = -\Gamma(M_j d\ddot\theta + B_j d\dot\theta + K_j d\theta) \tag{7}$$

where $\tau_{\text{joint}} \in \Re^m$ is the additional joint control torque for controlling the joint impedance; $M_j, B_j, K_j \in \Re^{m\times m}$ are the desired joint inertia, viscosity and stiffness, respectively; and $d\theta = \theta - \theta_d \in \Re^m$ is the deviation vector between the joint angle θ and the equilibrium joint angle θ_d. The matrix $\Gamma \in \Re^{m\times m}$ filters out the joint torque in such a way that the filtered joint torque has no effect on the end-effector acceleration [14], [15]

$$\Gamma = I - \bar J(\bar J)^+ \tag{8}$$

where $(\bar J)^+$ denotes the pseudoinverse of $\bar J$. It can be easily shown that the additional joint control torque τ_{joint} satisfies the following condition

$$\bar J^T \tau_{\text{joint}} = 0 \tag{9}$$

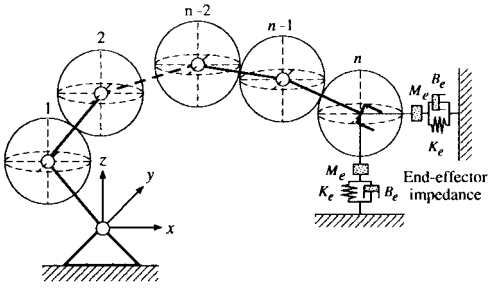

(a)

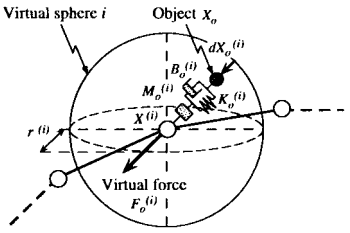

(b)

Fig. 1. Schematic representation of the noncontact impedance control (NCIC).

such that τ_{joint} has no dynamic effect on the end-effector motion of the manipulator, and the end-effector impedance remains as the desired one given by (2).

III. Noncontact Impedance Control

Fig. 1 shows a schematic representation of the noncontact impedance control. Let us consider the case where an object approaches a manipulator. In order to consider the interaction between the whole arm and the object without contact, a number of virtual spheres with radius $r^{(i)} (i = 1,2,\ldots,n)$ are used, the center of each being located on a link or a joint of the manipulator as shown in Fig. 1(a). Then, when the object comes into the interior of the virtual sphere i, the normal vector from the surface of the sphere to the object is given as

$$dX_o^{(i)} = X_r^{(i)} - r^{(i)} a^{(i)} \tag{10}$$

where $X_r^{(i)} = X_o - X^{(i)}$ is the displacement vector from the center of the sphere $X^{(i)} \in \Re^l$ to the object $X_o \in \Re^l$. Also, the vector $a^{(i)} \in \Re^l$ is defined as

$$a^{(i)} = \begin{cases} \dfrac{X_r^{(i)}}{\left|X_r^{(i)}\right|} & \left(\left|X_r^{(i)}\right| \neq 0\right) \\ 0 & \left(\left|X_r^{(i)}\right| = 0\right) \end{cases} \tag{11}$$

where $|X_r^{(i)}|$ denotes the Euclidian norm of $X_r^{(i)}$. When the object is in the virtual sphere, $|X_r^{(i)}|$ is less than $r^{(i)}$.

Next, the virtual noncontact impedance is considered between the object and the center of the virtual sphere, as shown in Fig. 1(b), where $M_o^{(i)}, B_o^{(i)}$, and $K_o^{(i)}$ represent the virtual inertia, viscosity and stiffness matrices associated with the ith virtual sphere, respectively. Using the noncontact impedance and the displacement vector $dX_o^{(i)}$, the virtual external force $F_o^{(i)} \in \Re^l$ exerted from the object to the center of the sphere

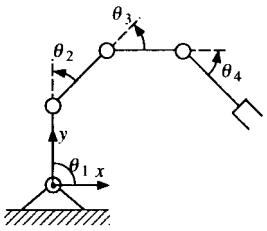

Fig. 2. A four-joint planar manipulator.

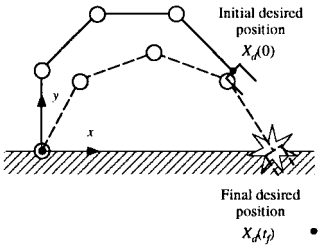

Fig. 3. An example of a contact task.

is defined as

$$F_o^{(i)} = \begin{cases} M_o^{(i)} d\ddot{X}_o^{(i)} + B_o^{(i)} d\dot{X}_o^{(i)} + K_o^{(i)} dX_o^{(i)} & \left(\left|X_r^{(i)}\right| < r^{(i)}\right) \\ 0 & \left(\left|X_r^{(i)}\right| \geq r^{(i)}\right). \end{cases} \tag{12}$$

It can readily be seen from (11) and (12) that $F_o^{(i)}$ becomes zero when the object is not in the virtual sphere or the object exists at the center of the sphere.

The virtual external force defined above can be transformed to the equivalent joint torque $\tau_o^{(i)}$

$$\tau_o^{(i)} = J^{(i)\mathrm{T}} F_o^{(i)} \tag{13}$$

where $J^{(i)}$ denotes the Jacobian matrix associated with the center of the ith virtual sphere. For the virtual sphere n defined at the end-effector, the virtual external force $F_o^{(n)}$ is directly incorporated in the motion equation of the end-effector (2)

$$M_e d\ddot{X} + B_e d\dot{X} + K_e dX = F_{\text{ext}} + F_o^{(n)}. \tag{14}$$

Consequently, by revising (6) the noncontact impedance control law is given as

$$\tau = \tau_{\text{effector}} + \tau_{\text{comp}} + \tau_{\text{joint}} + \tau_o^{(n)} + \{(1-\alpha)I + \alpha\Gamma\} \sum_{i=1}^{n-1} \tau_o^{(i)} \tag{15}$$

where α is the parameter which can adjust the effect of the noncontact impedance to the end-effector motion. When $\alpha = 1$, the virtual force $F_o^{(i)} (i = 1, 2, \ldots, n-1)$ does not affect the end-effector motion. However, when $\alpha = 0$, the end-effector motion is changed by the virtual external force applied to the whole arm as well as to the end-effector. In addition to the end-effector impedance control, the relative motion between the manipulator and its environment can be considered through the virtual impedance $M_o^{(i)}, B_o^{(i)}, K_o^{(i)}$ using the noncontact impedance control.

IV. Computer Simulations

Computer simulations using a four-joint planar manipulator, as shown in Fig. 2, were carried out. The parameters of each link of the manipulator were as follows: the length was 0.4 m, the mass 3.75 kg, the moment of inertia 0.8 kgm^2, and the center of mass of each link was at its middle point. The end-effector impedance of the manipulator was determined as $M_e = \text{diag.}[1, 1]$ kg, $B_e = \text{diag.}[20, 20]$ Nm/s, $K_e = \text{diag.}[100, 100]$ N/m, and the desired end-effector position, i.e., the equilibrium position, was simply chosen at its initial position, where the initial posture of the manipulator was $\theta(0) = [\frac{\pi}{2}, -\frac{\pi}{4}, -\frac{\pi}{4}, -\frac{\pi}{4}]^T$ rad. Also the desired joint impedance in (7) was chosen as $M_j = \text{diag.}[0.01, 0.01, 0.01, 0.01]$ kgm^2, $B_j = \text{diag.}[0.2, 0.2, 0.2, 0.2]$ Nm/(rad/s), and $K_j = \text{diag.}[1, 1, 1, 1]$ N/rad, and the equilibrium joint angle θ_d as its initial value $\theta(0)$. The parameter α in (15) was $\alpha = 1$ except for the computer simulation shown in Fig. 11(b). The parameters included in the control law should be designed according to the given task.

A. Application to Contact Task

Let us consider a case where the manipulator collides with the environment (Fig. 3). By using the conventional impedance control only, an impact force arises [18]. Therefore, the noncontact impedance between the end-effector and its environment is used to reduce the impact force.

The characteristics of the environment are represented using an impedance model such as

$$M_w \ddot{X} + B_w \dot{X} + K_w (X_s - X) = F_{\text{ext}} \tag{16}$$

where X_s represents the equilibrium position of the environment and M_w, B_w, and K_w are the inertia, viscosity, and stiffness of the environment, respectively. Note that $F_{\text{ext}} = 0$ when the end-effector is not in contact with the object. In this simulation, $M_w = \text{diag.}[0, 0.5]$ kg, $B_w = \text{diag.}[0, 100]$ Ns/m and $K_w = \text{diag.}[0, 10\,000]$ N/m are used, and the surface of the object is located along the x axis (Fig. 3).

Fig. 4 shows the simulation result of the contact task under the conventional impedance control, where: (a) the end-effector trajectory $X(t)$ in the x-y plane, (b) the time histories of the end-effector trajectory $y(t)$, and (c) the interaction force $F_{\text{ext}}(t)$ in the y direction are shown. The desired trajectory $X_d(t)$ of the end-effector was determined by using the fifth-order polynomial under the boundary conditions of

$$X_d(0) = \left(\frac{1+\sqrt{2}}{5}, 0.2\right) \text{ m}$$
$$X_d(t_f) = \left(\frac{2+\sqrt{2}}{5}, -0.2\right) \text{ m}$$
$$\dot{X}_d(0) = (0, 0) \text{ m/s}$$
$$\dot{X}_d(t_f) = (0, 0) \text{ m/s}$$
$$\ddot{X}_d(0) = (0, 0) \text{ m/s}^2$$
$$\ddot{X}_d(t_f) = (0, 0) \text{ m/s}^2$$

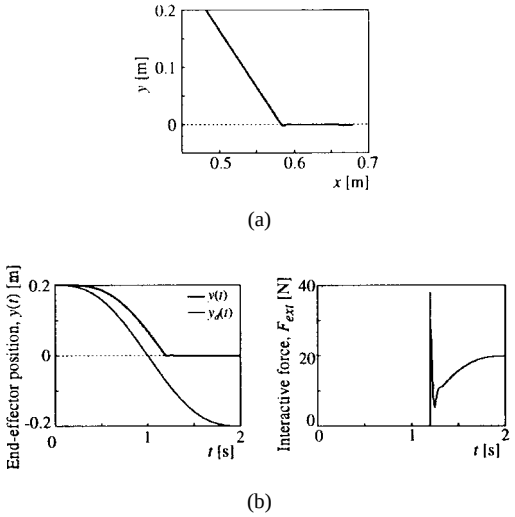

Fig. 4. A simulation result of the contact task under the conventional impedance control.

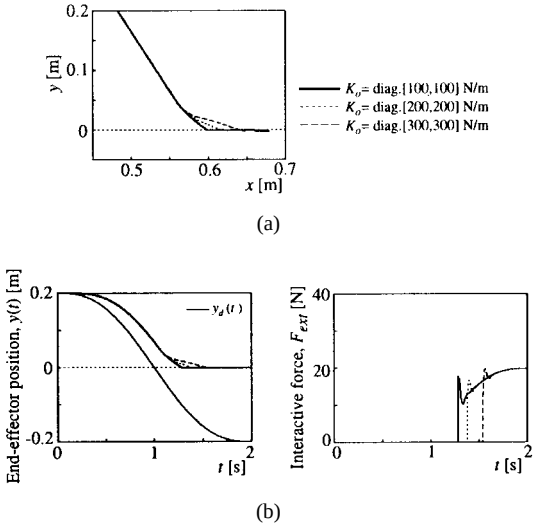

Fig. 5. Simulation results of the contact task under the NCIC. Three different virtual stiffness matrices are used.

where $t_f = 2$ s. The computation of the manipulator dynamics was performed by using Appel's method [19], and the sampling time for control was 1 ms.

By contrast, Figs. 5 and 6 show the results under the noncontact impedance control. The virtual circle with a radius $r^{(1)} = 0.3$ m was used only for the end-effector $(n = 1)$, and the point X_o was determined on the surface of the object in such a way that dX_o in (12) always becomes a normal vector to the object, so that X_o is the closest point on the surface of the object from the end-effector. In Fig. 5, the virtual stiffness $K_o^{(1)}$ was changed as $K_o^{(1)} = \text{diag.}[100, 100], \text{diag.}[200, 200], \text{diag.}[300, 300]$ N/m; whereas constant inertia and viscosity $M_o^{(1)} = \text{diag.}[0.5, 0.5]$ kg and $B_o^{(1)} = \text{diag.}[10, 10]$ Ns/m were used. Also in Fig. 6, the virtual viscosity was changed as $B_o^{(1)} = \text{diag.}[10, 10], \text{diag.}[50, 50], \text{diag.}[90, 90]$ Ns/m with constant inertia and stiffness $M_o^{(1)} = \text{diag.}[0.5, 0.5]$ kg and $K_o^{(1)} = \text{diag.}[0, 0]$ N/m.

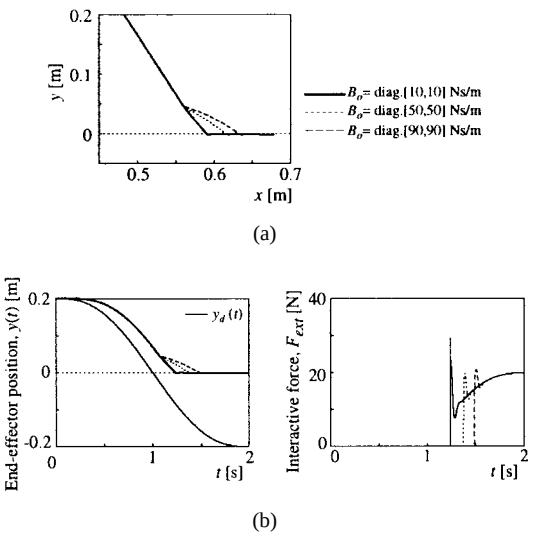

Fig. 6. Simulation results of the contact task under the NCIC. Three different virtual viscosity matrices are used.

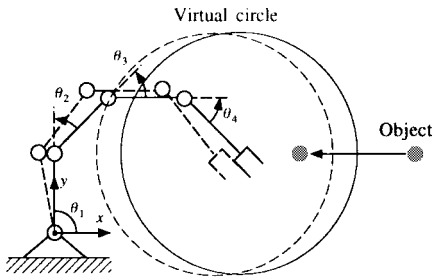

Fig. 7. Avoidance of an object using the NCIC.

In Fig. 4, a large impact force is observed when the end-effector collides with the object. On the contrary, in Figs. 5 and 6, the end-effector slows down before contact, so that the impact force decreases considerably. It can be seen, then, that the virtual external force acts to the end-effector in the direction of avoiding the collision with the object.

B. Application to Object Avoidance

Next, let us consider the manipulator close to a moving object. By using the conventional impedance control only, the manipulator cannot take any action in avoiding the object without the interaction force.

As an example of the noncontact impedance control, a virtual circle was attached to the end-effector $(n = 1)$ as shown in Fig. 7. Time histories of the end-effector trajectory $x(t)$ and the object trajectory $x_o(t)$ in the x direction are shown in Fig. 8, where the radius of the sphere was $r^{(1)} = 0.3$ m. The virtual stiffness was changed as $K_o^{(1)} = \text{diag.}[0, 0], \text{diag.}[50, 50], \text{diag.}[100, 100]$ N/m with constant inertia and viscosity $M_o^{(1)} = \text{diag.}[0.5, 0.5]$ kg, $B_o^{(1)} = \text{diag.}[10, 10]$ Ns/m. The object was oscillating in a cosine form for the period of 2 s and with the amplitude of 0.3 m in the direction of x axis as shown in Fig. 8. When the distance between the end-effector and the object was more than $r^{(1)}$, the end-effector did not move. However, when the object

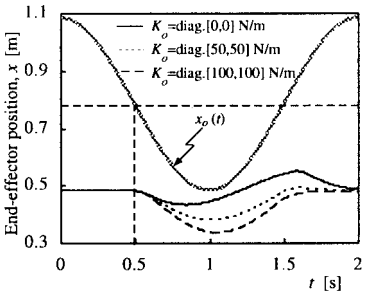

Fig. 8. Change of the end-effector trajectories for a moving object under the NCIC.

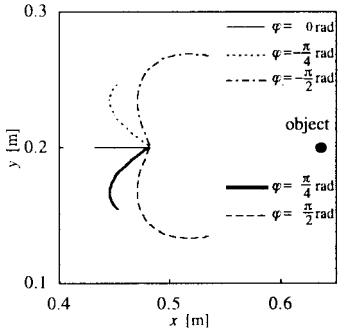

Fig. 9. Control of the end-effector trajectories via the noncontact impedance matrices.

came into the virtual circle, the end-effector was displaced in the direction opposite the object. As well, the trajectories of the end-effector reflected the stiffness between the end-effector and the object.

After this, the noncontact impedance matrices $M_o^{(1)}$, $B_o^{(1)}$, $K_o^{(1)}$ were changed to be

$$M_o^{(1)} = 0.5R(\varphi) \text{ kg}$$
$$B_o^{(1)} = 10R(\varphi) \text{ Ns/m}$$
$$K_o^{(1)} = 50R(\varphi) \text{ N/m}$$
$$R(\varphi) = \begin{pmatrix} \cos\varphi & -\sin\varphi \\ \sin\varphi & \cos\varphi \end{pmatrix}$$

and the step response of the end-effector was examined, where the object was located at a position with a distance of 0.15 m apart from the initial position of the end-effector in the direction of the x axis. According to the rotation matrix $R(\varphi)$, the direction of the virtual external force was rotated with the angle φ in a counterclockwise direction.

Fig. 9 shows the change of the step responses of the end-effector with the angle φ. The response of the end-effector, that is, the amplitude and the direction, can be controlled by regulating the noncontact impedance matrices.

As another example of noncontact impedance control, eight virtual circles were used $(n = 8)$, as shown in Fig. 10, where the centers of the circles were located at the middle point of each link and at each joint except for the first joint.

Fig. 11 shows the change of the arm posture for a moving object. The radius of each circle was $r^{(i)} = 0.1$ m, and the virtual impedance of $M_o^{(i)} = \text{diag.}[2, 2]$ kg, $B_o^{(i)} = \text{diag.}[40, 40]$ Ns/m, and $K_o^{(i)} = \text{diag.}[200, 200]$ were used. The parameter

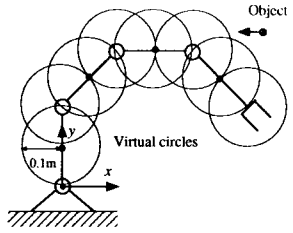

Fig. 10. A manipulator and virtual circles.

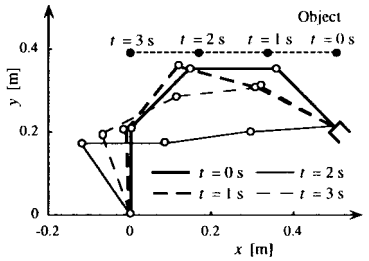

(a)

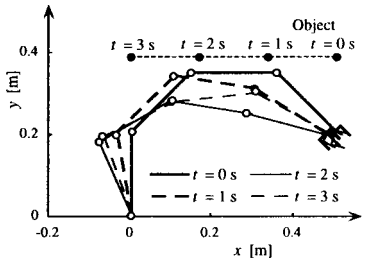

(b)

Fig. 11. Avoidance of an object using the NCIC.

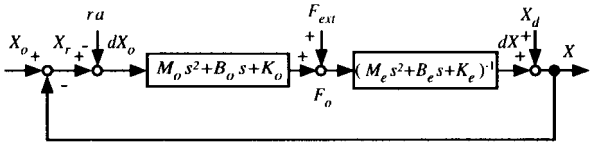

Fig. 12. The block diagram of the NCIC.

α in (15) was $\alpha = 1$ in Fig. 11(a) in order to utilize the arm redundancy, while $\alpha = 0$ was used in Fig. 11(b). It can be seen from both figures that the manipulator moves without contact and that the parameter α can specify the use of the arm redundancy.

C. Virtual Impedance Parameters

As shown in Fig. 8, the dynamic response of the manipulator to the object's motion is highly dependent on both the virtual impedance and the end-point impedance. In this subsection, we analyze the effect of the virtual impedance to the end-point dynamic response.

The block diagram of the system including the end-point virtual impedance as shown in Fig. 8 is given in Fig. 12. The motion equation of the end-point of the manipulator can be

derived by substituting (12) into (14) as follows:

$$Md\ddot{X} + Bd\dot{X} + KdX = \tilde{F} \tag{17}$$

$$\begin{aligned}\tilde{F} = F_{\text{ext}} &+ M_o(\ddot{X}_o - \ddot{X}_d - r\ddot{a}) \\ &+ B_o(\dot{X}_o - \dot{X}_d - r\dot{a}) \\ &+ K_o(X_o - X_d - ra)\end{aligned} \tag{18}$$

where $M = M_e + M_o^{(1)}$, $B = B_e + B_o^{(1)}$ and $K = K_e + K_o^{(1)}$. For simplicity, we assume that the vector a is constant. This gives

$$\frac{X(s)}{X_o(s)} = (Ms^2 + Bs + K)^{-1}(M_o s^2 + B_o s + K_o) \tag{19}$$

where $X(s)$, $X_o(s)$ denote the Laplace transform of $X(t)$, $X_o(t)$, respectively. Therefore we can see that the dynamic response of the end-point is determined by the sum of the virtual impedance and the end-point impedance. In Fig. 8, for example, the case of $K_o^{(1)} = \text{diag.}[0, 0]$ N/m, indicated by the solid line, resulted in an overdamped response. Therefore, the end-point followed the object going away from the end-point, so that the large overshoot was observed after the object went out of the virtual sphere.

The end-point impedance parameters M_e, B_e, and K_e should be determined according to a task. Therefore, we discuss how the virtual impedance parameters can be designed with a consideration for the overall system characteristics in mind (19). For simplicity, let us consider the following positive definite matrices as the end-point impedance:

$$M_e = T^T \tilde{M}_e T \tag{20}$$

$$B_e = T^T \tilde{B}_e T \tag{21}$$

$$K_e = T^T \tilde{K}_e T \tag{22}$$

where $T \in \Re^{l \times l}$ is the nonsingular matrix, each column of which corresponds to an eigenvector; and $\tilde{M}_e, \tilde{B}_e, \tilde{K}_e \in \Re^{l \times l}$ are the diagonal matrices, each diagonal element of which is an eigenvalue of the corresponding impedance matrices, respectively.

For simplicity, we chose the following virtual impedance matrices:

$$M_o^{(1)} = T^T \tilde{M}_o T \tag{23}$$

$$B_o^{(1)} = T^T \tilde{B}_o T \tag{24}$$

$$K_o^{(1)} = T^T \tilde{K}_o T. \tag{25}$$

The problem, then, is how to design the eigenvalues of the virtual impedance matrices. As an example, the eigenvalues of $\tilde{B}_o$ and $\tilde{K}_o$ are determined as follows:

$$\tilde{B}_{oj} = 2\omega_n^j \zeta^j (\tilde{M}_{ej} + \tilde{M}_{oj}) - \tilde{B}_{ej} \tag{26}$$

$$\tilde{K}_{oj} = (\omega_n^j)^2 (\tilde{M}_{ej} + \tilde{M}_{oj}) - \tilde{K}_{ej} \tag{27}$$

where $\tilde{B}_{oj}$, $\tilde{K}_{oj}$ are the jth diagonal elements of $\tilde{B}_o$, $\tilde{K}_o$, respectively; and ζ^j, ω_n^j are the damping ratio and the natural frequency for the corresponding degree of the freedom, respectively. It should be noted that it is not necessary for the eigenvalues defined as (26) and (27) to be positive, because the stability of the system is determined by the sum of the virtual impedance and the end-point impedance described by (19).

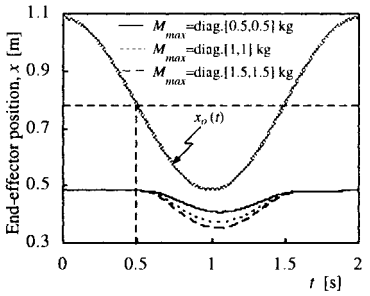

Fig. 13. Change of the end-effector trajectories for the moving object, where $\zeta^j = 1$ and $\omega_n^j = 10$ rad/s $(i = 1, 2)$ were used.

For the jth diagonal element of the virtual inertia, $M_o^{(1)}$ is also defined as

$$\tilde{M}_{oj} = \frac{\left|dX_o^{(1)}\right|}{r} M_{\max}^j \tag{28}$$

where $M_{\max}^j$ is the upper limit of the virtual inertia in the corresponding degree of the freedom. When the object comes into contact with the surface of the virtual sphere, the virtual inertia is automatically set to be small. As the object approaches the end-point, the virtual inertia becomes larger. Using (26)–(28), we can control the dynamic response of the end-point to the object motion according to the object position, as well as by the given end-point impedance.

Fig. 13 shows examples of the simulation results using (26), (27), and (28), where the upper limit of the virtual inertia $M_{\max}^j$ were changed as $M_{\max}^j = 0.5, 1.0, 1.5$ kg $(j = 1, 2)$. As well, the constant damping ratio and the natural frequency were also used: $\zeta^j = 1$ and $\omega_n^j = 10$ rad/s $(j = 1, 2)$. Other simulation conditions were the same as the ones used in Fig. 8. Note that the matrix T is the unit matrix, since the given end-point impedance matrices are diagonal. From the figure, it can be seen that the end-point returns to its initial position without overshooting, as specified by the damping ratio. The changes of the virtual impedance parameters are also shown in Fig. 14, where the parameters are adaptively regulated according to the object motion.

V. Experiments

A. Experimental Apparatus

The experiment of the noncontact impedance control was carried out using a direct-drive robot (a three-joint planar type, KOBELCO) and a PSD camera system to measure the position of the object, as shown in Fig. 15. Table I shows the link parameters of the robot. The task space was the horizontal plane; and an LED was attached at the tip of a stick in order to represent the point object, where the measurement error was less than ± 3 mm in the task space. The computation of the control law was performed by using four CPU's (Transputer, T800, 25 MHz).

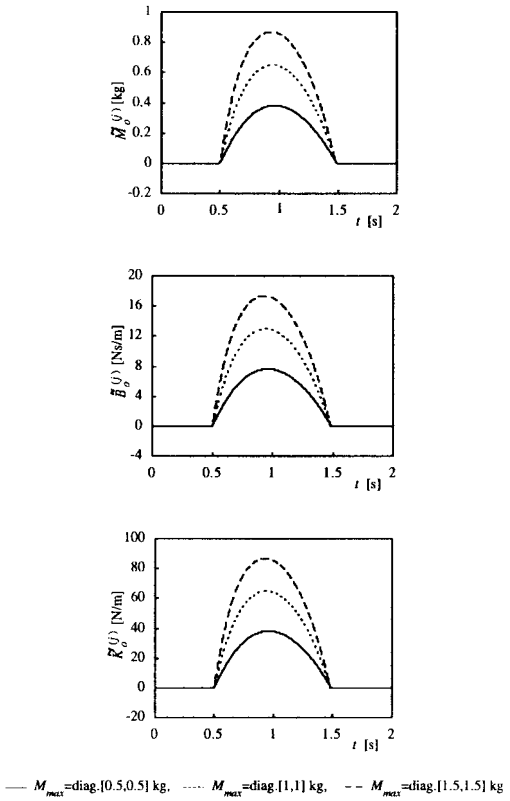

Fig. 14. Time histories of the virtual impedance parameters.

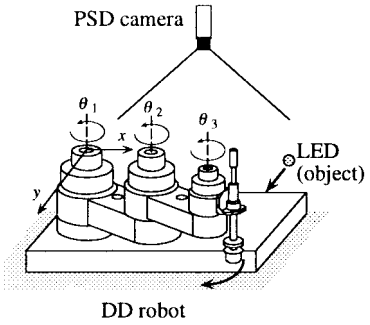

Fig. 15. Experimental apparatus.

TABLE I
LINK PARAMETERS OF THE ROBOT

	Link 1	Link 2	Link 3
Length (m)	0.25	0.25	0.125
Mass (kg)	20.8	13.2	8.84
Center of mass (m)	0.064	0.065	0.031
Moment of inertia (kgm^2)	0.334	0.196	0.0851
Joint friction (Nms/rad)	2.69	1.88	0.0634

B. Robust Impedance Control

The impedance control cannot regulate the end-effector impedance perfectly without an accurate model of the robot dynamics. Also, unexpected external disturbances are often applied to the robot, so that errors between the desired impedance and the realized one may arise. Therefore, we need to develop

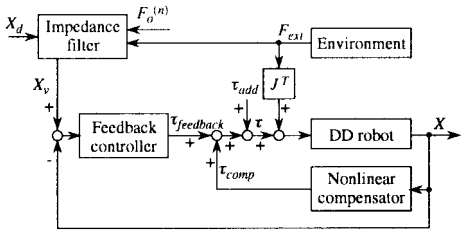

Fig. 16. Robust impedance control of a direct-drive robot in the presence of modeling error.

a robust impedance control, within the presence of modeling errors, for the experiments using the direct-drive robot.

The impedance controller used in this experiment is divided into two parts, as shown in Fig. 16: the impedance filter and the robust position controller.

1) Impedance Filter: This part computes the ideal trajectory of the end-effector X_v from the measured external force F_{ext}, the computed virtual external force $F_o^{(n)}$ and the desired end-effector impedance, which must be satisfied to realize the desired impedance

$$M_e\ddot{X}_v + B_e\dot{X}_v + K_eX_v = V_d \tag{29}$$

$$V_d = F_{\text{ext}} + F_o^{(n)} + M_e\ddot{X}_d + B_e\dot{X}_d + K_eX_d \tag{30}$$

where $X_v = [x_v^1, x_v^2, \ldots, x_v^l]^T$, and $V_d = [v_d^1, v_d^2, \ldots, v_d^l]^T \in \Re^{\mathcal{N}}$ denotes the modified total disturbance force. Since the initial values of $X_v, \dot{X}_v, \ddot{X}_v$ are known and the desired end-effector impedance M_e, B_e, K_e and the desired (equilibrium) position $X_d, \dot{X}_d, \ddot{X}_d$ are given, X_v can be solved numerically based on the measured and computed forces F_{ext} and $F_o^{(n)}$ in real time.

2) Robust Position Controller: Using the ideal trajectory of the end-effector X_v, the state feedback controller is designed. Transforming the motion equation (1) of the manipulator into the task space, we have

$$M_x(\theta)\ddot{X} + \mu_x(\theta,\dot{\theta}) = F + F_{\text{ext}} \tag{31}$$

where $\mu_x(\theta,\dot{\theta}) = (M^{-1}(\theta)J^TM_x)^Th(\theta,\dot{\theta}) - M_x\dot{J}\dot{\theta} \in \Re^{\mathcal{N}}$; and $F \in \Re^{\mathcal{N}}$ is the equivalent end-effector force generated by τ. The end-effector control force F is defined as follows:

$$F = \hat{M}_x(\theta)a^* + \hat{\mu}_x(\theta,\dot{\theta}) - F_{\text{ext}} \tag{32}$$

$$a^* = M_e^{-1}V - M_e^{-1}B_e\dot{X} - M_e^{-1}K_eX \tag{33}$$

where $V = [v^1, v^2, \ldots, v^l]^T \in \Re^{\mathcal{N}}$ is the new input signal; and $\hat{M}_x(\theta)$ and $\hat{\mu}_x(\theta,\dot{\theta})$ are the estimated values of $M_x(\theta)$ and $\mu_x(\theta,\dot{\theta})$, respectively.

If there is no modeling error in the robot dynamics, we can easily obtain the ideal end-effector motion equation by substituting (32) and (33) into (31):

$$M_e\ddot{X} + B_e\dot{X} + K_eX = V \tag{34}$$

since $\hat{M}_x(\theta) = M_x(\theta)$ and $\hat{\mu}_x = \mu_x$. Therefore, comparing (34) with (29), we can see that the input signal V should be determined by V_d of (30). For a real robot, however, the modeling error such as uncertainties in the estimated

parameters, that is, $\hat{M}_x(\theta) \neq M_x(\theta)$ and $\hat{\mu} \neq \mu_x$, and unexpected external disturbances always exists. As a result, the error $E_m = [E_m^1, E_m^2, \ldots, E_m^l]^T \in \Re^l$ from the ideal motion equation (34) arises as

$$M_e\ddot{X} + B_e\dot{X} + K_eX = V + E_m. \tag{35}$$

Our goal is to find the control input V in (33) in such a way that the resulted end-effector motion equation (35) under the control input V reduces to (29). Kuo and Wang [20] proposed the robust position feedback control in the task space based on the following simple model of the error signal E_m:

$$[E_m]^{(p)} = \sum_{j=1}^{p} b_j [E_m]^{(p-j)} \tag{36}$$

where $[E_m]^{(p)}$ denotes the pth time derivative of E_m. In this paper, assuming $p = 1$ and $b_1 = 0$ for simplicity, we adopt this model and derive the following state equation from (29), (35), and (36):

$$\dot{Z} = LZ + MS \tag{37}$$

$$e = NZ \tag{38}$$

where $Z = [e, \dot{e}, \ddot{e}]^T \in \Re^{3l}$ and $e = X - X_v$. Also,

$$S = \dot{E}_V \tag{39}$$

$$E_V = V - V_d \tag{40}$$

$$L = \begin{bmatrix} 0 & I & 0 \\ 0 & 0 & I \\ 0 & -M_e^{-1}K_e & -M_e^{-1}B_e \end{bmatrix} \in \Re^{3l\times 3l} \tag{41}$$

$$M = \begin{bmatrix} 0 & 0 & M_e^{-1^T} \end{bmatrix}^T \in \Re^{3l\times l} \tag{42}$$

$$N = [I \quad 0 \quad 0] \in \Re^{l\times 3l} \tag{43}$$

where $I \in \Re^{l\times l}$ and $0 \in \Re^{l\times l}$ denote the unit matrix and the zero matrix, respectively.

For the state equations (37) and (38), we apply the state feedback control

$$S = -KZ \tag{44}$$

where $K = [K_1, K_2, K_3] \in \Re^{l\times 3l}$ is the feedback gain matrix which should be chosen in such a way that Z in (37) converges to zero faster than the change of X_v. If we choose the diagonal matrix for $K_i = \text{diag.}[k_i^1, k_i^2, \ldots, k_i^l] \in \Re^{l\times l}$, $k_i^j > 0$, we have the following equations from (39) and (44):

$$\dot{E}_V = -K_1e - K_2\dot{e} - K_3\ddot{e}. \tag{45}$$

Therefore, we can compute the control input V in (33) from (40) and (45)

$$V = E_v + V_d \tag{46}$$

$$E_v = -K_1\int_0^t edt - K_2e - K_3\dot{e}. \tag{47}$$

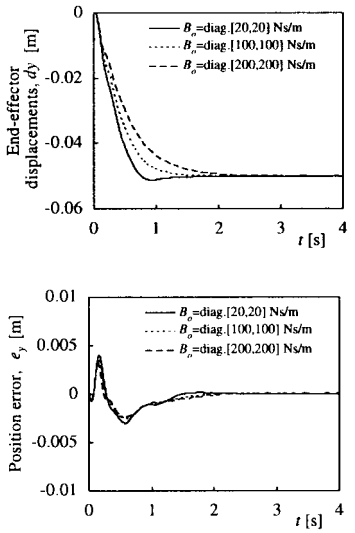

Fig. 17. Step responses of the end-effector under the NCIC.

Consequently the impedance control law derived in this paper is summarized as follows:

$$\tau = \tau_{\text{feedback}} + \tau_{\text{comp}} + \tau_{\text{add}} \tag{48}$$

$$\tau_{\text{feedback}} = J^T(\hat{M}_x(\theta)a^* - F_{\text{ext}}) \tag{49}$$

$$\tau_{\text{comp}} = J^T\hat{\mu}_x(\theta, \dot{\theta}) + \hat{g}(\theta) \tag{50}$$

$$\tau_{\text{add}} = \tau_{\text{joint}} + \{(1-\alpha)I + \alpha\Gamma\}\sum_{i=1}^{n-1}\tau_o^{(i)}. \tag{51}$$

Under the above control law, the resulted end-effector trajectory X almost agrees with the ideal trajectory of the end-effector X_v computed by the impedance filter, so that the desired end-effector impedance can be realized. In the experiments, the feedback gain $K_i = \text{diag.}[13.5, 5.75, 0.925]$ $(i = 1, 2)$ is used, which results in the poles $P_i = [-6, -6, -6]$ $(i = 1, 2)$ of the closed loop system (37) with (44).

C. Experimental Results

The end-effector impedance parameters of the robot were: $M_e = \text{diag.}[25, 25]$ kg; $B_e = \text{diag.}[200, 200]$ Ns/m; $K_e = \text{diag.}[400, 400]$ N/m; and, the desired end-effector position was chosen as its initial one. In the impedance control method proposed in this paper, it is necessary to measure the accelerations of the joint angles and the LED [see (7) and (12)]. For digital differentiation, the low-pass first-order differentiation filter ${}_3f^3$ invented by Usui and Amidror [21] were used. For second-order differentiation, the first-order filter was applied twice in cascade. The sampling time for differentiation was 1 ms, while the one for control was 2.6 ms.

In Fig. 17, the virtual circle with its radius $r^{(1)} = 0.3$ m was used for the end-effector $(n = 1)$, and the step responses of the end-effector were measured, where the object was located at a position with a distance 0.2 m apart from the initial position of the end-effector in the direction of the y axis. The initial posture was $\theta(0) = [0.8, -1.02, -1.49]^T$ rad. Fig. 17(a) shows the experimental results of the step responses, where the virtual viscosity $B_o^{(1)}$ was changed to

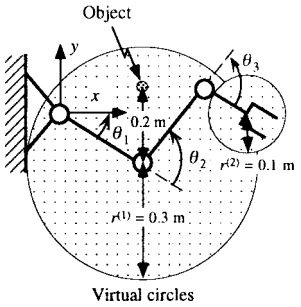

Fig. 18. The DD robot and the object.

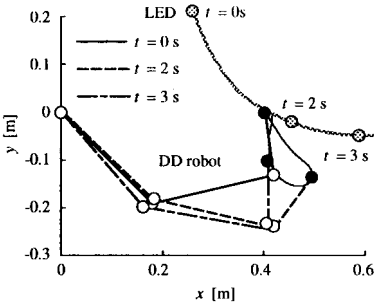

Fig. 21. The DD robot avoiding the object.

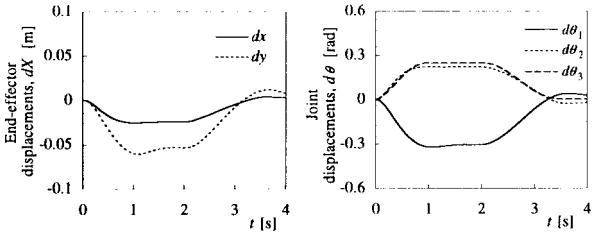

Fig. 19. Change of the arm posture under the NCIC with $\alpha = 0$.

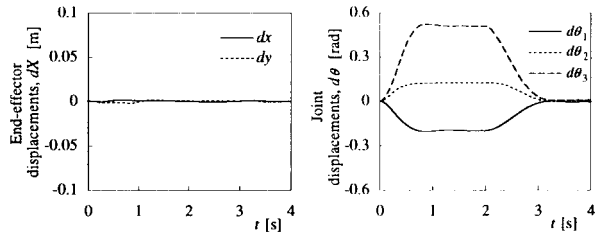

Fig. 20. Change of the arm posture under the NCIC with $\alpha = 1$.

$B_o^{(1)} = \text{diag.}[20, 20], \text{diag.}[100, 100], \text{diag.}[200, 200]$ Ns/m with constant inertia and stiffness $M_o^{(1)} = \text{diag.}[4, 4]$ kg, $K_o^{(1)} = \text{diag.}[400, 400]$ N/m. Also in Fig. 17(b), the error $e_y(t)$ between the measured trajectory X and the ideal end-effector trajectory X_v computed from (29) and (30) are shown corresponding to viscosity $B_o^{(1)}$. The step responses of the end-effector changed depending on $B_o^{(1)}$, while the control errors were almost constant and less than 0.004 m.

After this, the response of the arm for an object close to the second joint was examined. The virtual circles were set at the second joint and the end-effector with a radius $r^{(1)} = 0.3$ m and $r^{(2)} = 0.1$ m, as shown in Fig. 18. The initial posture $\theta(0) = [-0.56, 1.45, -1.43]^T$ rad was used as its equilibrium, that is, $\theta_d(t) = \theta(0)$. The object was located at a position with a distance 0.2 m apart from the initial end-effector position in the direction of the y axis at $t = 0$ s and was removed at $t = 2$ s. Figs. 19 and 20 show the results under $\alpha = 0$ and $\alpha = 1$ [see (15)], respectively, where (a) represents the end-effector displacements and (b) the joint displacements. Also, the virtual impedance parameters, $M_o^{(1)} = \text{diag.}[4, 4]$ kg; $B_o^{(1)} = \text{diag.}[80, 80]$ Ns/m; $K_o^{(1)} = \text{diag.}[400, 400]$ N/m, were used.

In the experiments, the joint impedance in (7) was chosen as $M_j = \text{diag.}[0.02, 0.02, 0.02]$ kgm^2, $B_j = \text{diag.}[0.9, 0.9, 0.9]$ Nm/(rad/s), and $K_j = \text{diag.}[2.0, 2.0, 2.0]$ Nm/rad. If the joint impedance (7) is not used, the arm posture does not return to its initial posture after the object is removed. Using the joint impedance and the parameter α, the kinematic redundancy is effectively utilized in the framework of the NCIC.

Finally, Fig. 21 shows the end-effector trajectory $X(t)$ for the moving object $X_o(t)$, where the virtual sphere was defined at the end-effector with the parameters $r^{(1)} = 0.2$ m; $M_o^{(1)} = \text{diag.}[4, 4]$ kg; $B_o^{(1)} = \text{diag.}[80, 80]$ Ns/m; and $K_o^{(1)} = \text{diag.}[400, 400]$ N/m. The posture of the robot changes according to the motion of the object.

VI. Conclusion

This paper has proposed the noncontact impedance control method which can control the virtual impedance between the manipulator and the environment in addition to the end-effector impedance. This method uses the virtual interaction force in order to express the relationship between the manipulator and the environment without contact, as a result, the dynamics of the relative motion of the manipulator to the object can be regulated. The validity and feasibility of the method were confirmed through computer simulation and robot experiments.

Generally speaking, there are many difficulties with vision-based robot control in three-dimensional (3-D) space, including measurements of the 3-D position of objects with occlusion and computational delay of the control system due to the video rate sampling. In the proposed method, however, visual information on the task space is required only for the interior of the virtual sphere. Therefore, instead of using a visual sensor like a camera system, 3-D position sensors such as a magnetic sensor and an ultrasonic sensor can be used. Also, if the object is occluded by other objects, the virtual impedance should be set to the occluding object.

This method includes a number of parameters such as: the location and the size of the virtual sphere; the joint and virtual impedance matrices; and, the parameter α for the use of the arm redundancy. Future research will be directed by how the parameters can be determined according to the given task and its environment.

References

[1] N. Hogan, "Impedance control: An approach to manipulation, parts i, ii, iii," *ASME J. Dyn. Syst., Meas., Contr.*, vol. 107, no. 1, pp. 1–24, 1985.

[2] N. Hogan, "Stable execution of contact tasks using impedance control," in *Proc. IEEE Int. Conf. Robotics Automation*, 1987, pp. 1047–1054.
[3] S. Tachi, T. Sakaki, H. Arai, S. Nishizawa, and J. F. Pelaez-Polo, "Impedance control of a direct-drive manipulator without using force sensors," *Adv. Robot.*, vol. 5, no. 2, pp. 183–205, 1991.
[4] E. Colgate and N. Hogan, "An analysis of contact instability in terms of passive physical equivalents," in *Proc. IEEE Int. Conf. Robotics Automation*, 1989, pp. 404–409.
[5] J. E. Agapakis, J. M. Katz, J. M. Friedman, and G. N. Epstein, "Vision-aided robotic welding: An approach and a flexible implementation," *Int. J. Robot. Res.*, vol. 9, pp. 17–33, Oct. 1990.
[6] B. Espiau, F. Chaumette, and P. Rives, "A new approach to visual servoing in robotics," *IEEE Trans. Robot. Automat.*, vol. 8, pp. 313–326, June 1992.
[7] R. Sharma, J. Y. Herve, and P. Cucka, "Dynamic robot manipulation using visual tracking," in *Proc. IEEE Int. Conf. Robotics Automation*, 1992, pp. 1844–1849.
[8] A. Castano and S. Hutchinson, "Visual compliance: Task-directed visual servo control," *IEEE Trans. Robot. Automat.*, vol. 10, pp. 334–342, June 1994.
[9] T. Arai, H. Ohta, and T. Suzuki, "Collision avoidance among multiple robots using virtual impedance," in *Proc. IEEE/RSJ Int. Workshop Intelligent Robot. Syst.*, 1989, pp. 479–485.
[10] M. Hatagi, H. Akamatsu, T. Tsuji, and M. Kaneko, "Non-contact impedance control for manipulators," in *Proc. JSME Annu. Conf. Robotics Mechatronics'96*, vol. B, pp. 853–856 (in Japanese).
[11] T. Tsuji, H. Akamatsu, M. Hatagi, and M. Kaneko, "Vision-based impedance control for robot manipulators," in *CD-ROM Proc. IEEE/ASME Int. Conf. Advanced Intelligent Mechatronics*, 1997.
[12] Y. Nakabo, I. Ishii, and M. Ishikawa, "Robot control using visual impedance," in *Proc. JSME Annu. Conf. Robotics Mechatronics'96*, vol. B, pp. 999–1002 (in Japanese).
[13] T. Tsuji, H. Akamatsu, and M. Kaneko, "Noncontact impedance control for redundant manipulators," in *Proc. 1997 IEEE Int. Conf. Robotics Automation*, pp. 2571–2576.
[14] O. Khatib, "A unified approach for motion and force control of robot manipulators: The operational space formulation," *IEEE J. Robotics Automation*, vol. RA-3, pp. 43–53, Feb. 1987.
[15] O. Khatib, "Motion/force redundancy of manipulators," in *Proc. Jpn.–U.S.A. Symp. Flexible Automation*, 1990, vol. 1, pp. 337–342.
[16] T. Tsuji and A. Jazidie, "Impedance control for redundant manipulators: An approach to joint impedance regulation utilizing kinematic redundancy," *J. Robot Soc. Jpn.*, vol. 12, no. 4, pp. 1072–1078, 1994 (in Japanese).
[17] T. Tsuji, A. Jazidie, and Makoto Kaneko, "Multi-point impedance control for redundant manipulators," *IEEE Trans. Syst., Man, Cybern. B*, vol. 26, pp. 707–718, Oct. 1996.
[18] T. Tsuji, K. Ito, and P. Morasso, "Neural network learning of robot arm impedance in operational space," *IEEE Trans. Syst., Man, Cybern. B*, vol. 26, pp. 290–298, Apr. 1996.
[19] V. Potkonjak and M. Vukobtatovic, "Two new methods for computer forming of dynamic equation of active mechanisms," *Mech. Mach. Theory*, vol. 14, no. 3, pp. 189–200, 1987.
[20] C. Y. Kuo and S. P. T. Wang, "Robust position control of robotic manipulator in Cartesian coordinates," *IEEE Trans. Robot. Automat.*, vol. 7, pp. 653–659, Oct. 1991.
[21] S. Usui and I. Amidror, "Digital low-pass differentiation for biological signal processing," *IEEE Trans. Biomed. Eng.*, vol. BME-29, pp. 686–693, Oct. 1982.

Toshio Tsuji was born in Kyoto, Japan, on December 25, 1959. He received the B.E., M.E., and Doctor of Engineering degrees 1982, 1985, and 1989, all from Hiroshima University, Hiroshima, Japan.

From 1985 to 1994, he was a Research Associate with the Faculty of Engineering, Hiroshima University, and from 1992 to 1993 was a Visiting Researcher at the University of Genova, Genova, Italy. He is currently an Associate Professor, Department of Industrial and Systems Engineering, Hiroshima University. He is interested in various aspects of motor control in robot and human movements. His current research interests have focused on the control of EMG-controlled prostheses, and computational neural sciences, in particular, biological motor control.

Dr. Tsuji is a member of Japan Society of Mechanical Engineers, Robotics Society of Japan, and Japanese Society of Instrumentation and Control Engineers.

Makoto Kaneko received the B.S. degree in mechanical engineering from Kyushu Institute of Technology, Japan, in 1976, and the M.S. and Ph.D. degrees in mechanical engineering from Tokyo University, Japan, in 1978 and 1981, respectively.

From 1981 to 1990 he was a Researcher with the Mechanical Engineering Laboratory (MEL), Ministry of International Trade and Industry (MITI), Tsukuba Science City, Japan. From 1988 to 1989, he was a Post-Doctoral Fellow at the Technical University of Darmstadt, Germany, where he joined a space robotics project. From 1990 to 1993, he was an Associate Professor of Computer Science and System Engineering at Kyushu Institute of Technology. From November 1991 to January 1992, he was an Invited Professor at the Technical University of Darmstadt. Since October 1993, he has been a Professor of Industrial Engineering Department at Hiroshima University, Hiroshima, Japan. His research interests include tactile-based active sensing, grasping strategy, sensor applications, and experimental robotics.

Dr. Kaneko received the Outstanding Young Engineer Award in 1983 from the Japan Society of Mechanical Engineers, the Best Paper Awards from the Robotics Society of Japan in 1994, and from the Japanese Society of Instrumentation and Control Engineers in 1996. He also received the Humboldt Research Award in 1997. He served as an Associate Editor of IEEE TRANSACTIONS ON ROBOTICS AND AUTOMATION from 1990 to 1994. He has been a program committee member for IEEE International Conference on Intelligent Robots and Systems since 1991. He also worked as a program committee member for the 1995, 1996, and 1998 IEEE International Conference on Robotics and Automation. He is a member of the IEEE Robotics and Automation Society, the IEEE Systems, Man, and Cybernetics Society, and the IEEE Industrial Electronics Society. He is also a member of Japan Society of Mechanical Engineers, Robotics Society of Japan, and Japanese Society of Instrumentation and Control Engineers.